MYC Family Amplification Dictates Sensitivity to BET Bromodomain Protein Inhibitor Mivebresib (ABBV075) in Small-Cell Lung Cancer

Joshua P. Plotnik[1], Zheng Zha[2], Weiguo Feng[2], Irene Lee[3], Jacob Riehm[3], Ryan A. McClure[4], Stephanie Sandoval[4], Tamar Uziel[3], Erin Murphy[2], Xin Lu[2], and Lloyd T. Lam[3]

ABSTRACT

Small-cell lung cancer (SCLC) accounts for nearly 15% of all lung cancers. Although patients respond to first-line therapy readily, rapid relapse is inevitable, with few treatment options in the second-line setting. Here, we describe SCLC cell lines harboring amplification of *MYC* and *MYCN* but not *MYCL1* or non-amplified *MYC* cell lines exhibit superior sensitivity to treatment with the pan-BET bromodomain protein inhibitor mivebresib (ABBV075). Silencing *MYC* and *MYCN* partially rescued SCLC cell lines harboring these respective amplifications from the antiproliferative effects of mivebresib. Further characterization of genome-wide binding of MYC, MYCN, and MYCL1 uncovered unique enhancer and epigenetic preferences.

Implications: Our study suggests that chromatin landscapes can establish cell states with unique gene expression programs, conveying sensitivity to epigenetic inhibitors such as mivebresib.

Introduction

Small-cell lung cancer (SCLC) accounts for nearly 15% of all lung cancers (1) and is established from basal lung neuroendocrine precursors upon inactivation of the p53 and RB1 tumor suppressor genes (2). First-line therapy, cisplatin/carboplatin plus etoposide, often demonstrates partial response followed by rapid relapse (2). The advanced stage of diagnosis and rapid progression of SCLC is responsible for poor 5-year survival (3). Despite these clinical challenges, recent work characterizing the molecular and genetic landscapes has led to a greater understanding of key transcription factor drivers of molecular subtypes in SCLC, offering novel avenues for targeted therapeutic intervention (4).

In >20% of SCLC patient tumors and >50% of human-derived cell lines, an amplification event occurs in any of the three MYC transcription factors: *MYC*, *MYCN*, or *MYCL1* (5–7). These MYC family member amplification events occur in a mutually exclusive fashion and result in the overexpression of a single MYC transcription factor in tumors and cell lines. Further, MYC, MYCN, or MYCL1 expression is required for tumor growth in small-cell cancers. Previous efforts to identify the roles of MYC, MYCN, and MYCL1 have relied on transcriptome analysis of cell lines harboring amplifications, demonstrating imbalanced apoptotic processes (8). *In vitro* evidence suggests that the three transcription factors target the canonical palindromic E-box motif, CACGTG. However, technical limitations have prevented the analysis of genome-wide binding of MYC, MYCN, and MYCL1 in SCLC (9). Understanding the programs driven by MYC family members in SCLC is critical for treating the disease with clinical compounds.

Targeting transcriptional addiction in cancers driven by MYC deregulation has been of increased focus over the past decade. Recent studies demonstrate the *in vitro* efficacy of bromodomain inhibitors in MYC-addicted cancers such as *IGH1-MYC* amplified multiple myeloma, *MYCN*-amplified neuroblastoma, and various leukemias and lymphomas (10, 11). The pan-BET inhibitor, mivebresib (ABBV075), inhibits the bromodomain containing proteins BRD2, BRD3, BRD4, and BRDT, demonstrating activity primarily in hematological cancers compared with solid tumors (12). However, single-agent activity was demonstrated in SCLC models with the ability to synergize with the BCL2 inhibitor, venetoclax (13).

Here, we demonstrate that SCLC cell lines harboring amplification of *MYC* and *MYCN* but not *MYCL1* exhibit superior sensitivity to treatment with mivebresib. We characterize the epigenetic and transcriptomic landscape of SCLC lines displaying sensitivity to mivebresib (ABBV075). We show for the first time, a direct comparison of MYC, MYCN, and MYCL1 genome-wide target binding, uncovering unique enhancer binding preferences for the three transcription factors determined by chromatin accessibility. Our study indicates that chromatin landscapes are critical in governing the unique functions of MYC family member transcription factors and are responsible for establishing gene expression programs conveying sensitivity or resistance to epigenetic inhibitors such as mivebresib.

Materials and Methods

Cell lines, antibodies, and compounds

All cell lines were originally obtained from ATCC, DSMZ, ECACC, or internal stocks and maintained by a Core Cell Line Facility that performed routine testing for mycoplasma using the

[1]Oncology Discovery Research, AbbVie Inc., North Chicago, Illinois. [2]Genomic Research Center, AbbVie Inc., North Chicago, Illinois. [3]Precision Medicine, Translational Oncology, AbbVie Inc., North Chicago, Illinois. [4]Physical Chemistry, Discovery, AbbVie Inc., North Chicago, Illinois.

Current address for Z. Zha: Takeda, Cambridge, Massachusetts; current address for W. Feng: Daiichi Sankyo, Inc., Basking Ridge, New Jersey; current address for X. Lu: Aster Insights, Hudson, Florida; and current address for R.A. McClure: Chan Zuckerberg Biohub, Chicago, Illinois.

Corresponding Author: Lloyd T. Lam, 1 North Waukegan Road, AP9A, North Chicago, IL 60064-6098. E-mail: lloyd.lam@abbvie.com

Mol Cancer Res 2024;22:689–98

doi: 10.1158/1541-7786.MCR-23-0599

MycoAlert Detection Kit (Lonza, Walkersville, MD) and authentication by short tandem repeat (STR) analysis using the Gene Print10 kit (Promega, Madison, WI). All cell lines were grown in Gibco RPMI-1640 + 10% FBS (ThermoFisher, Waltham, MA). The antibodies used in this study were as follows: MYCL1 (Abcam, cat# A304-796A), MYCN (Cell Signaling, Danvers, MA, cat# 51705), MYC (Cell Signaling, Danvers, MA, cat# 5605), H3K27Ac (Cat # 39133, Active Motif, Carlsbad, CA), and Alpha-Tubulin clone DM1A (Sigma, cat# T9026). ABBV075 (mivebresib) was synthesized by AbbVie, and JQ1 was purchased from Selleck Chemicals (Houston, TX).

siRNA reverse transfection

ON-TARGET plus siRNAs were obtained from Horizon Discovery, Inc. (Boulder, CO). siRNAs were introduced into the cells by reverse transfection using Lipofectamine RNAiMAX according to the manufacturer's instructions (Invitrogen, Carlsbad, CA). In brief, siRNAs were mixed with Lipofectamine RNAiMAX in Opti-MEM (Invitrogen) and dispensed in 96-well tissue culture plates. Cells were added at 1.5 to 2.5 $\times$ 10^4 cells/100 μL to a final concentration of 20 nmol/L siRNA. In experiments where ABBV075 was added to siRNA-containing lines, the cells were grown in a medium for 24 hours before compound addition. The cells were assayed for viability 72 hours after transfection with or without ABBV075, as described below.

Protein immunoblotting

Cell lysates were prepared in RIPA buffer (ThermoFisher Scientific, Waltham, MA) supplemented with cOmplete protease inhibitor cocktail tablets (Sigma-Aldrich, St. Louis, MO), and total protein was measured by the Bradford method. Equal amounts of protein were resolved in 4% to 20% Tris-Gly gels (Bio-Rad, Hercules, CA) and blotted with the antibodies described above. Following incubation with IR-conjugated secondary antibodies, membranes were imaged on an Odyssey CLx Imager (LiCOR Biosciences, Lincoln, NE).

Cell viability assays

Cells were plated onto 96- or 384-well plates in their respective culture medium and incubated at 37°C in an atmosphere of 5% CO_2. After overnight incubation, a serial dilution of compounds was prepared and added to the plate. The cells were further incubated for 3 or 5 days, and the CellTiter-Glo assay (Promega, Madison, WI) was then performed according to the manufacturer's instructions to determine cell viability. The luminescence signal from each well was acquired using the Enspire plate reader (PerkinElmer, Akron, OH), and the data were analyzed using GraphPad Prism software (GraphPad Software Inc, La Jolla, CA).

Motif searching and ontology analysis

Enriched motif searching was accomplished using the regulatory sequence analysis tools (RSAT) "peak motifs" platform (http://rsat.sb-roscoff.fr/). The settings for motif enrichment using RSAT were as follows: Discover overrepresented words and words with local overrepresentation at an oligomer length of 6, 7, and 8. The number of motifs returned per algorithm was set to 10. Ontology searches were performed using g:Profiler (http://biit.cs.ut.ee/gprofiler/). The settings for g:Profiler ontology algorithm were as follows: output style—textual, max functional category—1,500, significant only. All other settings remained as the default. Significance is shown as a corrected *P*-value.

Chromatin immunoprecipitation and sequencing

Cells were treated as described and then fixed for 10 minutes with direct addition of 1% formaldehyde (ThermoFisher, Waltham, MA). The fixation was stopped with 0.125 mmol/L glycine (Sigma-Aldrich, St. Louis, MO) for 5 minutes, followed by wash and collection in cold PBS and subsequent lysis (1% SDS, 10 μmol/L ethylenediaminetetraacetic acid (EDTA), 50 μmol/L Tris-Cl pH 8.0, 5 mmol/L sodium butyrate, cOmplete protease inhibitor cocktail tablets; Sigma-Aldrich, St. Louis, MO). Chromatin was sheared to 300 to 500 kb using the Bioruptor (Diagenode, Denville, NJ). Lysates were mixed 1:4 with dilution buffer (0.01% SDS, 1.1% Triton X-100, 1.2 μmol/L EDTA, 16.7 μmol/L Tris-Cl pH 8.0, 167 μmol/L NaCl, 5 mmol/L sodium butyrate, protease inhibitor cocktail tablet). Immunoprecipitation was completed for 4 hours with Dynabeads M280 Sheep Anti-Rabbit IgG (ThermoFisher, 11203D). Chromatin immunoprecipitation (ChIP) was washed once with Tris-EDTA (TE) and 3x with Wash Buffer (100 mmol/L Tris-Cl pH 8.0, 500 mmol/L LiCl, 15 Igepal, 1% deoxycholic acid) supplemented with phenylmethylsulfonylfluoride (PMSF). Beads were resuspended in Elution Buffer (20 mmol/L $NaHCO_3$, 1% SDS, 150 mmol/L NaCl), and cross-links were reversed overnight at 65°C, followed by 1-hr RNase A and proteinase K digestion at 45°C. DNA was purified using ChIP DNA Clean & Concentrator (Zymo).

ChIP sequencing data analysis

Processed ChIP sequencing (ChIP-seq) datasets by model-based analysis of ChIP-seq (MACS) were further analyzed using the USeq platform for intersecting regions and neighboring gene identifications (http://useq.sourceforge.net/). Further analysis of aligned bam files was conducted using NGSPlot (https://github.com/shenlab-sinai/ngsplot) to visualize heatmaps and generate average profile plots. For each heatmap and average profile plot, the center of each peak was determined and extended 250 bp in the plus and minus directions to create the best window. Data could be accessed at the gene expression omnibus (GEO) accession number GSE230649.

Motif searching and ontology analysis

Motif searching was enriched using the RSAT "peak motifs" platform (http://rsat.sb-roscoff.fr/). The settings for motif

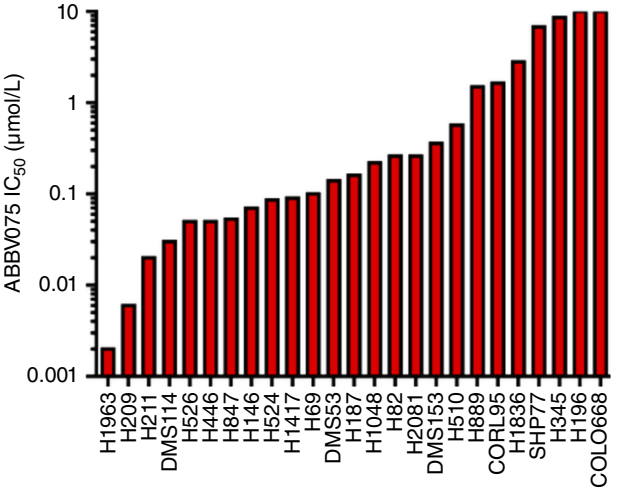

Figure 1.

In vitro cellular activity of mivebresib (ABBV075) in SCLC cell lines measured after 72 hours of treatment with the compound. IC_{50} is determined from three independent biological replicates.

enrichment using RSAT were as follows: Discover overrepresented words and words with local overrepresentation at an oligomer length of 6, 7 and 8. The number of motifs returned per algorithm was set to 10. Ontology searches were conducted using g:Profiler (http://biit.cs.ut.ee/gprofiler/). The settings for the g:Profiler ontology algorithm were as follows: output style—textual, max functional category—1,500, significant only. All other settings remained as the default. Significance is shown as a corrected *P*-value.

ATAC: sequencing and analysis

In brief, 50K viable cells were flow sorted (FACS AriaII) on ice, and transposase reactions were conducted as described (14). The assay for transposase-accessible chromatin and ChIP samples were sequenced by Illumina HiSeq, with single-end sequencing for ChIP-seq and paired-end sequencing for assay for transposase-accessible chromatin using sequencing (ATAC-seq). Sequence quality was assessed using the FastQC method. The sequences from the ChIP and input samples were aligned to human reference genome hg19 using Burrows–Wheeler aligner (BWA), and alignment metrics were calculated using Picard and samtools. A mapping blacklist from homer/encode was used to further filter the alignment.

Narrow peaks, for example, the transcription factor binding peaks, were detected using macs2 with default cutoff parameters.

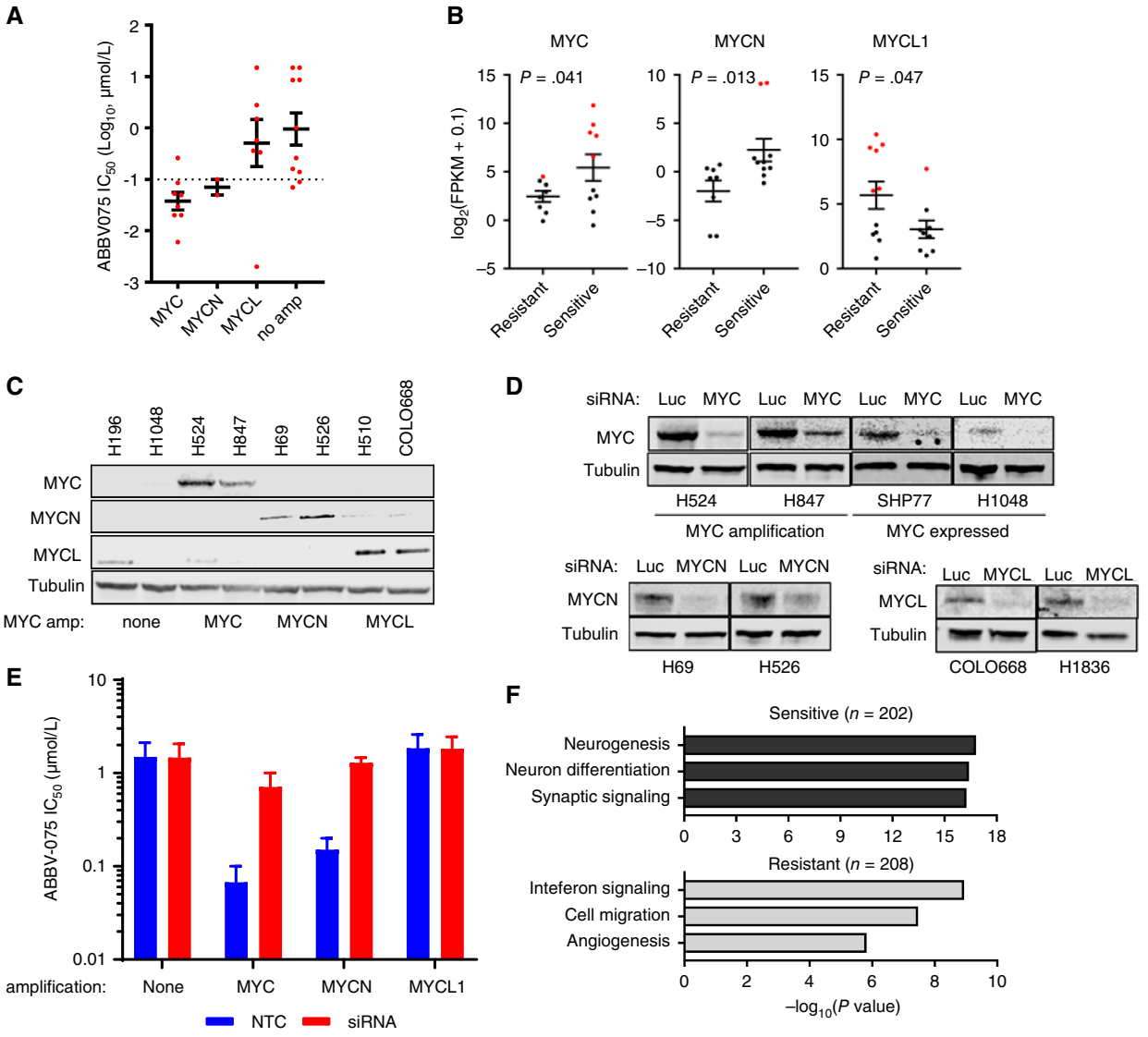

Figure 2.

MYC or *MYCN* but not *MYCL1* amplification correlates with mivebresib sensitivity. **A,** ABBV075 IC_{50} of SCLC cell lines grouped by MYC family member amplification status. No amp category refers to cell lines that do not harbor MYC, MYCN, and MYCL1 amplification. **B,** Expression of MYC family member genes classified into resistant and sensitive SCLC cell lines. Data points are red if CNV > 3 of a given MYC gene. **C,** Western blot of MYC, MYCN, and MYCL across SCLC cell lines. Tubulin is used as the loading control. **D,** Western blot confirmation of knockdown at 72 hours in representative cell lines. **E,** Viability values of *MYC*, *MYCN*, *MYCL1* amplified lines and non-amplified lines with respective siRNA after 72 hours treatment of ABBV075. Viability is measured by Cell Titer Glo. **F,** Gene ontology analysis of the 202 genes upregulated in ABBV075 sensitive cell lines and the 208 genes upregulated in ABBV075 resistant cell lines ranked by $-\log_{10}$(*P*-value).

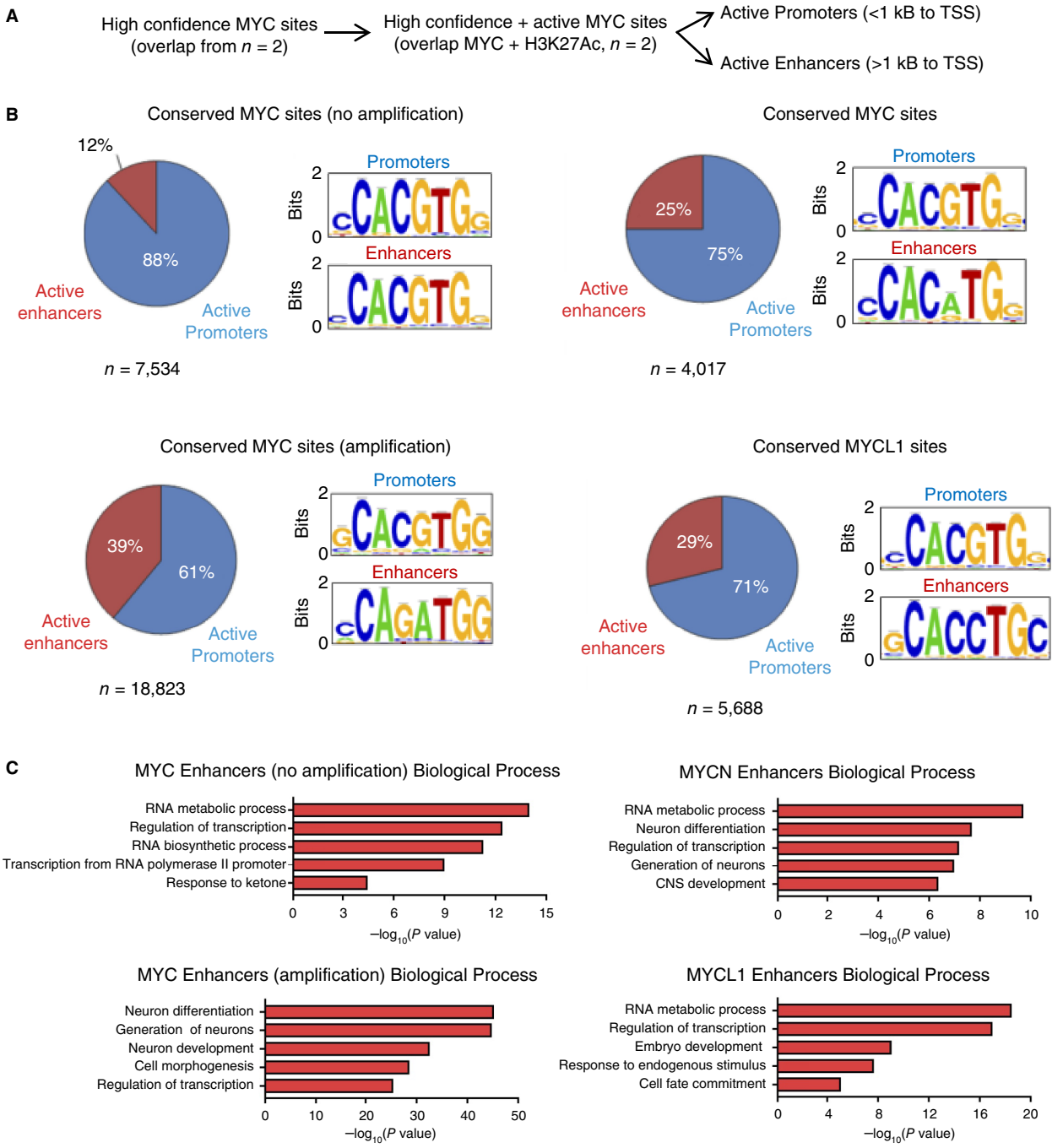

Figure 3.

Genome-wide localization of MYC family members unearths unique enhancer E-box elements. **A,** Schematic demonstrating the identification of high-confidence and active MYC, MYCN, and MYCL1 binding regions in representative SCLC cell lines. **B,** Pie chart demonstrating percentage of bound regions in MYC, MYCN, and MYCL1 data sets located near the transcriptional start site (TSS; active promoters, blue, <1 kb) or distal from start sites (active enhancers, red, >1 kb). Top E-box motif enriched in active promoter and enhancer data sets shown. **C,** Gene ontology analysis of the genes near high-confidence MYC bound regions in amplified cell lines in promoter or enhancer bins, ranked by $-\log_{10}$(*P*-value). (*Continued on the following page.*)

Broad peaks, for example, the epigenetic markers such as H3K27ac and BET binding, were detected using the broad peak option in macs2. False positives during peak detection were controlled using the FDR < 0.05 criterion. Overlapping peaks from replicated samples were detected using the R package Peakdiff.

Genome browser tracks such as alignment tracks, coverage tracks by bedgraph/bigwig, and peak tracks were also generated, and NGSPlot

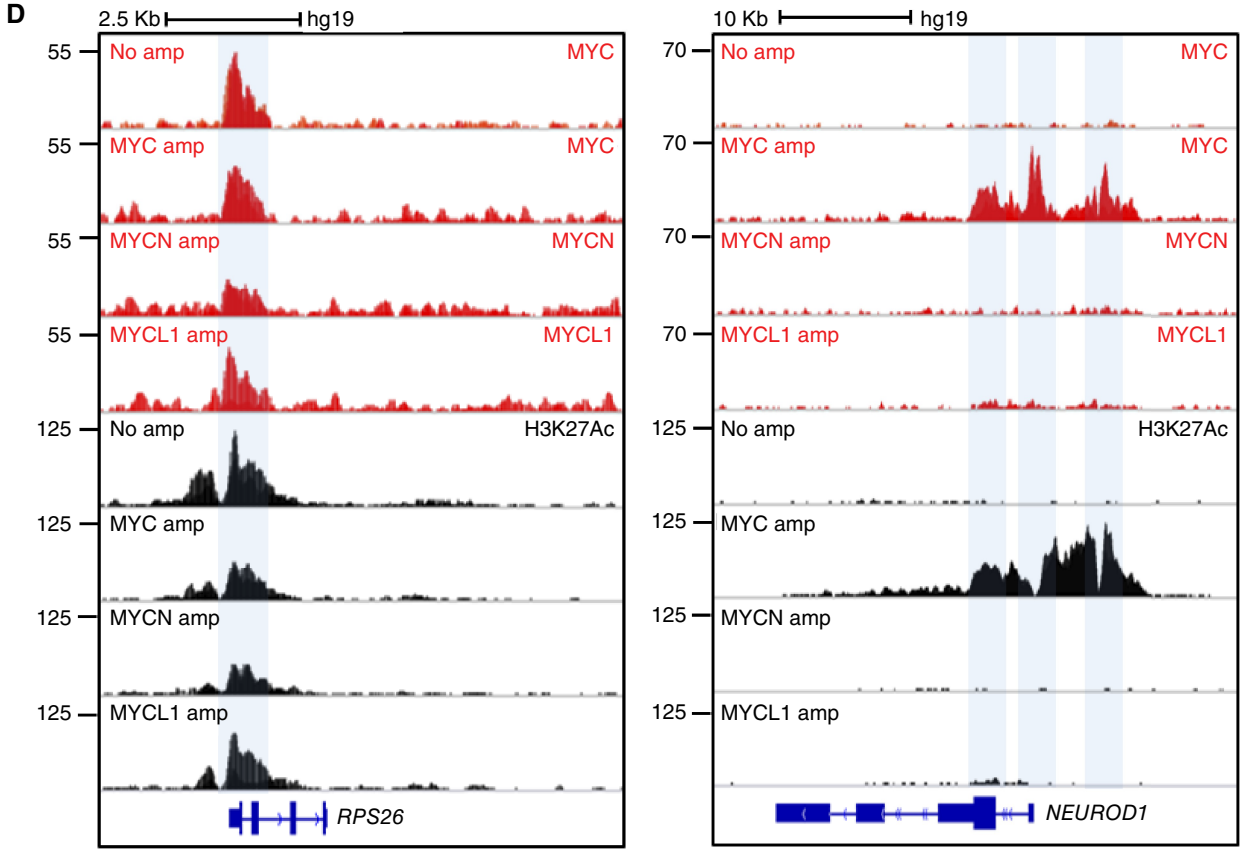

Figure 3.
(*Continued.*) **D,** Genome-browser view of a redundant MYC, MYCN, and MYCL1 bound region near the RPS26 promoter and a MYC amplification specific MYC bound region near the NEUROD1 gene.

was used to plot peak enrichment at or near various genomic locations such as promoters and enhancers. Data could be accessed at GEO accession GSE230649.

Results

MYC and *MYCN*, but not *MYCL1* amplification, correlate with mivebresib sensitivity

Previously, we showed that a subset of SCLC cell lines is sensitive to the BET inhibitor mivebresib alone, whereas other SCLC cell lines are sensitive to a combination of mivebresib and the BCL2 inhibitor venetoclax (13). Here, we sought to further understand the determinants of single-agent sensitivity to mivebresib. We first treated 25 SCLC cell lines with varying concentrations of mivebresib and measured viability after treatment for 3 days. We observed varying IC_{50} concentrations, ranging from 30 nmol/L to >10 μmol/L (**Fig. 1**), indicating cell line-specific sensitivity to BET inhibition. We also treated these cell lines with varying concentrations of another BET inhibitor, JQ1. Although mivebresib and JQ1 showed high correlations in response, (Pearson r = 0.9613; Supplementary Fig. S1A), mivebresib was more potent than JQ1 across the cell lines tested. To further understand potential biological pathways that underlie sensitivity to mivebresib, we used an IC_{50} cutoff of 100 nmol/L to separate SCLC into sensitive and resistant subgroups (12, 13).

It is well-documented that MYC-addicted cancers demonstrate sensitivity to BET inhibition; therefore, we sought to determine the role of MYC transcription factors in conferring sensitivity to mivebresib in SCLC cell lines. Interestingly, a strong correlation was observed between sensitivity to mivebresib and the amplification status of *MYC*, *MYCN*, or *MYCL1*. Seven of eight cell lines harboring *MYC* or *MYCN* amplification were sensitive (IC_{50} < 50 nmol/L), whereas 14/17 cell lines containing *MYCL1* or no *MYC* family member amplification had IC_{50} values > 100 nmol/L (**Fig. 2A**). Similarly, we observed a trend of higher gene expression of *MYC* and *MYCN* in the mivebresib-sensitive cell lines, whereas higher gene expression of *MYCL1* was observed in the mivebresib-resistant lines (**Fig. 2B**). We also observed higher protein expression of MYC and MYCN in the mivebresib-sensitive cell lines, whereas higher protein expression of MYCL1 was enriched in the mivebresib-resistant lines (Supplementary Fig. S2).

Role of MYC and MYCN in modulating sensitivity to mivebresib

To determine whether MYC and MYCN are responsible for driving sensitivity of SCLC cell lines to mivebresib, we evaluated the protein expression of MYC, MYCN, and MYCL in eight SCLC cell lines. Cell lines with amplification of *MYC*, *MYCN*, and *MYCL* expressed higher levels of MYC, MYCN, and MYCL protein, respectively (**Fig. 2C**). We then performed IC_{50} shift experiments by

transfecting siRNA against different MYC family members into cell lines harboring the respective amplification. Two cell lines were examined in each group (amplification of *MYC*, *MYCN*, and *MYCL1*, and no amplification) to limit cell line-specific variations. **Figure 2D** shows that the levels of MYC, MYCN, MYCL1 decreased upon silencing by their respective siRNA in these cell lines. The calculated IC_{50} was increased by approximately 10-fold in *MYC* (H524 and H847) and *MYCN* (H69 and H526) amplified cell lines upon silencing of *MYC* or *MYCN*. Meanwhile, there were no apparent changes in IC_{50} upon *MYCL1* silencing in *MYCL1* (Colo668 and H1836) amplified cell lines (**Fig. 2E**). Upon silencing *MYC*, IC_{50} values did not change in non-amplified MYC-expressing cell lines (NCI-H1048 and SHP77; **Fig. 2E**). This data suggest that *MYC* amplification is potentially functionally different from basal *MYC* expression. It should be noted that while *MYC* and *MYCN* knockdown affected the response to mivebresib, proliferation was not affected over 3 days (Supplementary Fig. S3). Taken together, *MYC* and *MYCN* amplification, but not *MYCL1* amplification, drives sensitivity to mivebresib in respective SCLC cell lines, insinuating divergent mechanisms between members of the MYC transcription factor family.

Differential expression analysis uncovers neuro-like phenotypes enriched in mivebresib-sensitive cell lines

SCLC has recently been classified into four distinct subtypes based on the expression of the transcription factors ASCL1, NEUROD1, POU2F3, or low expression of all three transcription factor signatures accompanied by an inflamed gene signature (15). Here, we determined whether sensitivity to mivebresib correlated with these SCLC subtypes. Interestingly, cell lines with high *NEUROD1* expression are more sensitive to mivebresib than cell lines with low *NEUROD1* (Supplementary Fig. S4A). Using a copy number variation (CNV) cutoff of >3 copies, we demonstrated that all SCLC cell lines in the Cancer Cell Line Encyclopedia (CCLE) database can be grouped into one of these subgroups (Supplementary Fig. S4B) and correlated with distinct neuroendocrine markers. *MYC* amplification correlated strongly with *NEUROD1* expression, whereas *MYCL1* positively correlated with *ASCL1*, consistent with other studies (16). Additionally, *MYC* amplification appeared distinct from *MYC* expression in the correlation with *NEUROD1*. While *MYC* amplification positively correlated with *NEUROD1* expression, *MYC*-expressing lines negatively correlated with *NEUROD1* expression (Supplementary Fig. S4B).

To further understand the potential biological pathways that underlie sensitivity to mivebresib, we used differential gene expression analysis of the sensitive versus the resistant cell lines (IC_{50} cutoff of 100 nmol/L) and identified that 202 genes significantly upregulated in sensitive cell lines (**Fig. 2F**). Interestingly, these genes are enriched in neuro-like biological processes such as neurogenesis, neuron differentiation, and synaptic signaling (**Fig. 2F**). In the resistant cell lines, 208 genes were significantly upregulated. These genes are involved in epithelial tumor-like programs such as migration and angiogenesis (**Fig. 2F**). Examples of upregulated genes in sensitive lines and resistant lines are shown in Supplementary Figs. S5A and S5B. The distinct enrichment of these gene expression programs in the sensitive and resistant groups suggests potential divergent transcriptional drivers in the response to mivebresib.

Genome-wide localization of MYC family members reveals unique preferences for enhancer E-box elements

A major limitation to understanding mechanisms among MYC family transcription factors is the lack of genome-wide localization data for MYC, MYCN, and MYCL1 in cell lines from similar tissue types. As SCLC harbors mutually exclusive amplification events of MYC family members, these cell lines offer a unique opportunity for addressing this issue. We performed chromatin immunoprecipitation followed by next-generation sequencing (ChIP-seq) of MYC, MYCN, and MYCL1 in amplified SCLC cell lines. We profiled two cell lines harboring the alteration for each amplification type (**Fig. 3A**). Each bound region data set was then overlapped within each group (e.g., *MYC* and *MYCN* amplification) to produce high-confidence binding sites in each amplification event. These high-confidence MYC, MYCN, and MYCL1 bound regions were overlapped with H3K27Ac marks to identify transcriptionally productive binding events throughout the genome (Supplementary Figs. S6A–S6D).

We identified 18,823 MYC, 4,017 MYCN, and 5,688 MYCL1 transcriptionally active bound regions genome-wide. Next, we determined whether the bound regions were proximal or distal to known transcriptional start sites. Using a cutoff of 1 kb, we showed that MYC family members primarily bind to promoters (61%–88%). However, we observed significant differences in the number of bound regions targeting enhancer regions in *MYC* amplification (39%) compared with *MYC*-expressing lines (12%; **Fig. 3B**). Interestingly, motifs (CACGTG) enriched in promoters were common between all MYC family members; however, the motif targeted in enhancer regions varied depending on cellular context (**Figs. 3B** and **C**). From motif enrichment analysis, we identified that MYC, MYCN, and MYCL1 preferentially target E-box motifs with a varied internal dinucleotide sequence. MYC preferentially targets CAGATG, MYCN targets CACATG, and MYCL targets CACCTG in the enhancer regions (**Fig. 3B**).

Next, we determined whether the central dinucleotide preferences observed between MYC family members occur near different classes of genes. Using ontology analysis, we observed that genes near active enhancers were involved in distinct biological processes compared with bound regions near active promoters (**Fig. 3C**; Supplementary Fig. S6E). Housekeeping functions, such as increased translation through RNA processing and ribosome biogenesis, were enriched in promoter elements near genes bound by all MYC family members. *RPS26*, a ribosomal gene, elicits this redundant promoter patterning (**Fig. 3D**). Interestingly, enhancers bound by MYC and MYCN in amplified cell lines demonstrated enriched neuroendocrine processes, represented by genes such as the neuroendocrine marker NEUROD1 in MYC amplified cell lines (**Fig. 3D**). Meanwhile, MYCL1 bound enhancers in amplified lines and no MYC amplified cell lines did not demonstrate enrichment in these pathways. Notably, the biological processes enriched in enhancers in *MYC*, *MYCN*, and *MYCL1* amplified lines align with biological functions of genes upregulated in mivebresib-sensitive or mivebresib-resistant SCLC cell lines (**Fig. 2F**), suggesting that the differential mechanisms of gene regulation by *MYC* amplification and response to therapeutic interventions are driven by non-canonical enhancer elements.

MYC and MYCN preferentially target a unique subset of neuroendocrine genes in SCLC through enhancer elements

As *MYC*- and *MYCN*-amplified SCLC cell lines exhibit sensitivity to BET inhibition, we sought to further compare the chromatin binding profiles among MYC, MYCN, and MYCL1. Of the nonredundant overlapped bound regions, we identified that 84% of MYCN regions fall within a MYC peak (**Fig. 4A**)

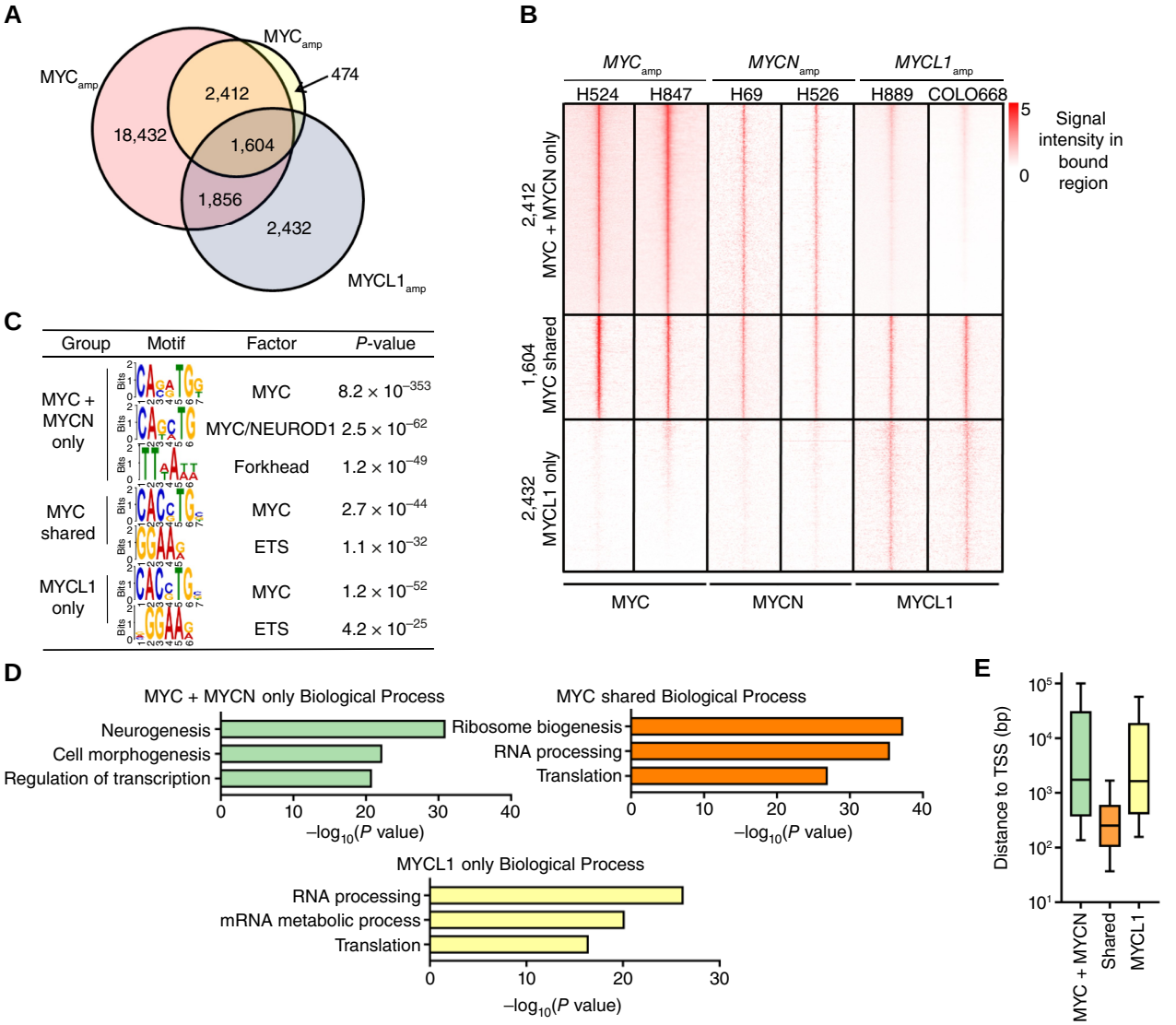

Figure 4.

MYC and MYCN target similar enhancers near genes involved in neuro-like phenotype. **A,** Venn diagram demonstrating the overlap of high-confidence MYC, MYCN, and MYCL1 binding regions from respective amplified cell lines. **B,** heatmap of MYC family member bound regions enrichment as determined in the Venn diagram in **A**. Bound regions indicated extended ±100 bp from the center of the peak with an extended window of 10 kb in either direction, normalized to each sample's genomic input by NGSPlot. **C,** Top enriched motifs in the bound regions in MYC + MYCN shared, MYC shared, and MYCL1-only bound region lists determined by RSAT peak motifs algorithms and ranked by the *P*-value. **D,** Gene otology analysis of the genes nearby regions as determined from **A** and depicted in the heatmap in **B**, ranked by $-\log_{10}$(*P*-value). **E,** Box plot showing the distance to TSS of the nearest gene for regions binned to MYC + MYCN shared, MYC shared, and MYCL1-only categories. The box denotes the 25th to 75th percentiles, and the horizontal bar depicts the median distance.

suggesting a common core set of genes regulated by MYC and MYCN (**Fig. 4B**). By contrast, the majority of MYCL1 bound regions did not overlap with either MYC or MYCN in their respective amplified setting (**Fig. 4A** and **B**), supporting our hypothesis that MYCL1 drives a mechanistically divergent role. To identify the genes near the MYC and MYCN core program, we ran gene ontology on three categories: MYC/MYCN, MYC shared, and MYCL1 only. Motif analysis recapitulated motifs identified in the individual data sets, promoting the hypothesis of unique E-box targeting by MYC and MYCN compared with MYCL (**Fig. 4C**). Identifying the nearest genes and running ontology analysis, we found that "MYC shared" bound regions appear near housekeeping genes, whereas bound regions commonly targeted by "MYC/MYCN" were associated with neurogenesis (**Fig. 4D**). We confirmed that the expansion of MYC binding sites was driven through the increased expression in amplified cell lines using MYC binding profiles in amplified versus MYC-expressed cell lines (Supplementary Figs. S7A–S7D). We next determined the location of the shared regions found in relation to the MYC/MYCN and MYCL1-only profiles.

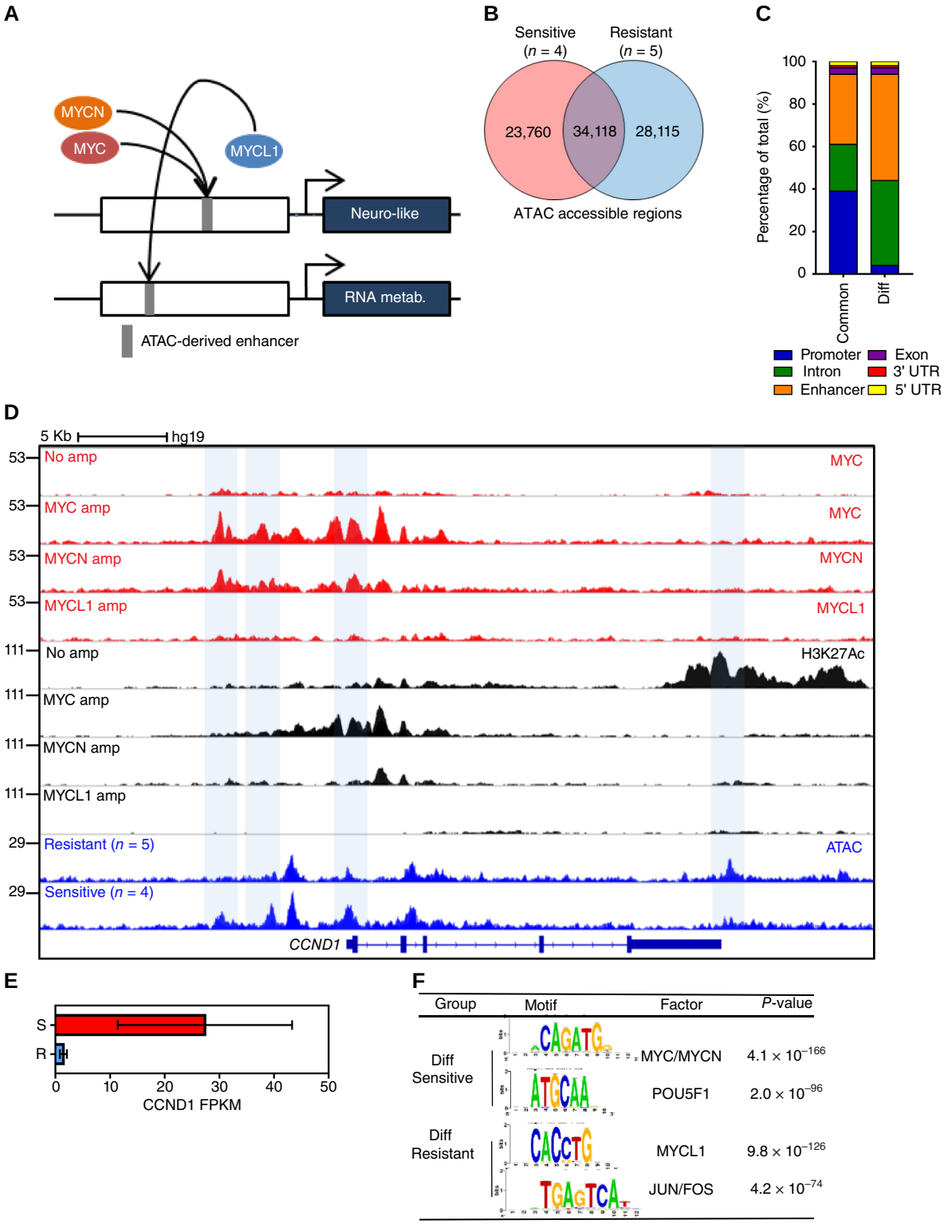

Figure 5.

Uniquely bound enhancer elements are regulated on the level of chromatin accessibility. **A,** Schematic showing MYC and MYCN targeting similar uniquely accessible enhancer regions driving genes involved in neuro-like phenotypes compared with enhancer accessibility targeted by MYCL1 as determined by ATAC-seq. **B,** Venn diagram displaying common and unique ATAC regions in SCLC cell lines sensitive ($n = 4$) and resistant ($n = 5$) to ABBV075. **C,** Interleaved bar plot showing the annotation of ATAC common and differential regions in major genomic categories. **D,** Representative (*Continued on the following page.*)

Consistent with our previous observations, "MYC shared" are, on average, 10 times closer to transcriptional start sites compared with "MYC/MYCN" or "MYCL1" programs (**Fig. 4E**). Further, principal component analysis of the H3K27Ac enhancer landscape and ATAC-seq showed that SCLC cell lines were clustered in closeness along PC1 by MYC amplification status (Supplementary Figs. S8A and S8B). Taken together, these data provide compelling evidence of core expression programs of distinct sets of genes regulated by MYC and MYCN but not MYCL1. However, how MYC transcription factors distinctly target unique enhancer E-box sequences remains unknown.

Uniquely bound enhancer elements are regulated on the level of chromatin accessibility

To address the observation that MYC, MYCN, and MYCL1 target unique E-box elements, we determined whether chromatin accessibility could explain preferentiality (**Fig. 5A**). We performed ATAC-seq on nine SCLC lines across the spectrum of sensitivity to mivebresib. Using our previous cutoff sensitivity of 100 nmol/L, we profiled four sensitive and five resistant cell lines for chromatin accessibility. Using MACS and combining ATAC-seq data sets in the two groups (sensitive and resistant), we identified a comparable amount of open chromatin in sensitive (57,878 regions) compared with resistant cell lines (62,233). Overlapping these accessible regions, we observed that the majority (34,118) of the regions were conserved between the two sets of cell lines (**Fig. 5B**). As we found that unique MYC binding sites occurred in enhancer elements, we sought to identify whether differentially accessible peaks between mivebresib-sensitive and mivebresib-resistant cell lines were also preferentially found in enhancer elements. Assigning peaks to features based on location to the nearest genes, we observed common accessible peaks primarily in promoters. Meanwhile, differentially accessible regions were found rarely in promoters (2.3%), most often in introns or enhancer regions genome-wide (**Fig. 5C**). *CCND1*, a gene significantly upregulated in sensitive cell lines and known to be repressed by BET inhibition, exhibits several differentially accessible regions in sensitive cell lines, which overlap with MYC and MYCN binding in an upstream and intronic enhancer (**Figs. 5D** and **E**).

Next, we determined if the differentially accessible regions could explain the divergence in MYC enhancer binding sites. Using these two groups, we identified significant enrichment for unique E-box elements in the sensitive and resistant groups. In each case, the top motifs matched previously identified E-box binding motifs for enhancer elements of MYC and MYCL1 (**Fig. 5F**). Furthermore, the second most enriched motifs also varied; sensitive lines demonstrated enrichment for POUF transcription factors, suggesting potential enrichment in tuft-cell lineage SCLC cell lines (17), whereas resistant lines showed enrichment for JUN/FOS family transcription factors, suggesting more epithelial-like functions as observed in gene ontologies from RNA-seq (**Fig. 5F**). Taking together, we propose that the mechanisms by which MYC, MYCN, and MYCL1 target noncanonical E-box enhancer elements is not driven by inherent differences in the DNA-binding abilities of each transcription factor but by the regulation of the chromatin landscape.

Discussion

In this study, we demonstrate that SCLC lines harboring amplification of *MYC* and *MYCN* but not *MYCL1* exhibit superior sensitivity to treatment with the bromodomain inhibitor mivebresib. Silencing *MYC* and *MYCN* partially rescued SCLC cell lines harboring these respective amplifications from the antiproliferative effects of mivebresib. Further characterization of genome-wide binding of MYC, MYCN, and MYCL1 uncovered unique enhancer and epigenetic preferences. Our study suggests that chromatin landscapes can establish cell states with unique gene expression programs, conveying sensitivity to epigenetic inhibitors such as mivebresib.

It has been shown that MYC transcriptional signatures increase following chemotherapy treatment in SCLC (18). This induction of MYC signature could be a resistance factor for chemotherapy as it was observed in genetically engineered mouse models that high expression of MYC or MYCN corresponds with poor response to chemotherapy (16, 19). It is highly possible that chemoresistant cells also acquire changes in the epigenetic landscape that drive differential cell states (20). To this end, we determined the roles of different MYC members by characterizing their binding sites and target genes. For the first time, we directly compare MYC, MYCN, and MYCL1 genome-wide binding and uncover unique enhancer binding preferences for the three transcription factors regulated by chromatin accessibility. Our study indicates that chromatin landscapes are critical for governing unique functions of MYC family member transcription factors responsible for the establishment of gene expression programs conveying sensitivity or resistance to mivebresib.

Our current model suggests that MYC and MYCN bind enhancers and exhibit signatures of neurogenesis, whereas MYCL regulates basal transcription (**Fig. 4D**). We hypothesize that these genes drive different cell states and their susceptibility to BET inhibition. While this concept is well-received in other tumor types, such as melanoma (21), this hypothesis needs to be further tested in small-cell neuroendocrine tumors (22). Interestingly, MYC drives the temporal evolution of SCLC subtypes by reprogramming neuroendocrine fate (23). We show that silencing *MYC* or *MYCN* rescues cells with these amplifications from BET inhibition but has no effect on cells with no or *MYCL* amplification. Our findings suggest the potential use of BET inhibitors in tumors with *MYC* or *MYCN* amplifications as a therapeutic option to test in rare indications. Future work will investigate the role of different pathways and genes downstream of *MYC* and *MYCN* amplification that leads to differential sensitivity to BET inhibition. For example, it is known that MYC-high cell lines and animal models exhibit better response to Aurora A/B kinase inhibitors (16, 24). Moreover, MYC-high SCLC is more apoptotically primed than MYC-low SCLC (25), proliferative, and glycolytic with unique metabolic vulnerabilities (16, 26).

One limitation of the current study is the lack of *in vivo* models. As the current study mainly focuses on the molecular mechanism by dissecting the chromatin landscape in these SCLC cell lines, we believe *in vivo* models would be outside the scope of this study.

(*Continued.*) genome browser demonstrating CCND1, an MYC and MYCN shared target gene, with uniquely accessible enhancer elements present in sensitive compared with resistant lines. Blue bars indicate regions of differential accessibility between groups. **E,** CCND1 gene expression in SCLC lines sensitive ($n = 11$, red) and resistant ($n = 14$, blue) to ABBV075, shown as fragments per kilobase per million (FPKM) values. **F,** Top enriched motifs in the bound regions are differentially accessible in the sensitive and resistant ATAC region lists as determined by RSAT peak motifs algorithms and ranked by the *P*-value.

Future studies will focus on generating genetically engineered mouse models to show further proof of concept. Taken together, our study demonstrates that SCLC cells harboring *MYC* and *MYCN* amplifications are more sensitive to BET inhibition and suggests a novel therapeutic strategy for patients with these genetic aberrations in SCLC.

Authors' Disclosures

J.P. Plotnik reports employment with AbbVie. I. Lee reports personal fees from AbbVie Inc outside the submitted work. X. Lu reports X. Lu reports previous employment with AbbVie and ownership of AbbVie stock. No disclosures were reported by the other authors.

Authors' Contributions

J.P. Plotnik: Conceptualization, resources, data curation, formal analysis, investigation, methodology, writing–original draft, writing–review and editing. **Z. Zha:** Resources, data curation, software, formal analysis, methodology. **W. Feng:** Resources, data curation, software, formal analysis, methodology. **I. Lee:** Resources, data curation, validation, investigation, writing–review and editing. **J. Riehm:** Investigation, methodology. **R.A. McClure:** Conceptualization, data curation, formal analysis, investigation, methodology. **S. Sandoval:** Data curation, formal analysis, investigation, methodology. **T. Uziel:** Conceptualization, writing–review. and editing. **E. Murphy:** Resources, data curation, software, formal analysis, methodology. **X. Lu:** Resources, data curation, software, formal analysis, supervision, methodology. **L.T. Lam:** Conceptualization, resources, data curation, supervision, writing–original draft, project administration, writing–review and editing.

Acknowledgments

We want to thank Translational Oncology and Oncology Discovery team members for their technical assistance and helpful discussions and Emily Faivre of AbbVie for critical review of the manuscript. We thank Tolga Turan and Josue Samayoa of AbbVie for their help with submitting data to GEO. J.P. Plotnik, I. Lee, T. Uziel, E. Murphy, S. Sandoval, J. Riehm, and L.T. Lam are employees of AbbVie and may hold AbbVie stock. Z. Zha, W. Feng, R.A. McClure, and X. Lu were employees of AbbVie at the time of the study and may hold AbbVie stock. AbbVie provided this research's design, study conduct, and financial support. AbbVie participated in the interpretation of data, review, and approval of the publication.

Note

Supplementary data for this article are available at Molecular Cancer Research Online (http://mcr.aacrjournals.org/).

Received July 27, 2023; revised March 28, 2024; accepted May 10, 2024; published first May 15, 2024.

References

1. van Meerbeeck JP, Fennell DA, De Ruysscher DKM. Small-cell lung cancer. Lancet 2011;378:1741–55.
2. Arcaro A. Targeted therapies for small cell lung cancer: where do we stand? Crit Rev Oncol Hematol 2015;95:154–64.
3. Bunn PA Jr., Minna JD, Augustyn A, Gazdar AF, Ouadah Y, Krasnow MA, et al. Small cell lung cancer: can recent advances in biology and molecular biology be translated into improved outcomes? J Thorac Oncol 2016;11:453–74.
4. Augert A, MacPherson D. Treating transcriptional addiction in small cell lung cancer. Cancer Cell 2014;26:783–4.
5. van der Hout AH, Kok K, van der Veen AY, Osinga J, de Leij LF, Buys CH. Localization of amplified c-myc and n-myc in small cell lung cancer cell lines. Cancer Genet Cytogenet 1989;38:1–8.
6. Little CD, Nau MM, Carney DN, Gazdar AF, Minna JD. Amplification and expression of the c-myc oncogene in human lung cancer cell lines. Nature 1983;306:194–6.
7. Meyer N, Penn LZ. Reflecting on 25 years with MYC. Nature 2008;8:976–90.
8. Kim YH, Girard L, Giacomini CP, Wang P, Hernandez-Boussard T, Tibshirani R, et al. Combined microarray analysis of small cell lung cancer reveals altered apoptotic balance and distinct expression signatures of MYC family gene amplification. Oncogene 2006;25:130–8.
9. Mukherjee B, Morgenbesser SD, DePinho RA. Myc family oncoproteins function through a common pathway to transform normal cells in culture: cross-interference by max and trans-acting dominant mutants. Genes Dev 1992;6:1480–92.
10. Shi J, Vakoc CR. The mechanisms behind the therapeutic activity of BET bromodomain inhibition. Mol Cell 2014;54:728–36.
11. Zeid R, Lawlor MA, Poon E, Reyes JM, Fulciniti M, Lopez MA, et al. Enhancer invasion shapes MYCN-dependent transcriptional amplification in neuroblastoma. Nat Genet 2018;50:515–23.
12. Bui MH, Lin X, Albert DH, Li L, Lam LT, Faivre EJ, et al. Preclinical characterization of BET family bromodomain inhibitor ABBV-075 suggests combination therapeutic strategies. Cancer Res 2017;77:2976–89.
13. Lam LT, Lin X, Faivre EJ, Yang Z, Huang X, Wilcox DM, et al. Vulnerability of small-cell lung cancer to apoptosis induced by the combination of BET bromodomain proteins and BCL2 inhibitors. Mol Cancer Ther 2017;16:1511–20.
14. Buenrostro JD, Wu B, Chang HY, Greenleaf WJ. ATAC-seq: a method for assaying chromatin accessibility genome-wide. Curr Protoc Mol Biol 2015;109:21.29.1–9.
15. Gay CM, Stewart CA, Park EM, Diao L, Groves SM, Heeke S, et al. Patterns of transcription factor programs and immune pathway activation define four major subtypes of SCLC with distinct therapeutic vulnerabilities. Cancer Cell 2021;39:346–60.e7.
16. Mollaoglu G, Guthrie MR, Bohm S, Bragelmann J, Can I, Ballieu PM, et al. MYC drives progression of small cell lung cancer to a variant neuroendocrine subtype with vulnerability to aurora kinase inhibition. Cancer Cell 2017;31:270–85.
17. Huang YH, Klingbeil O, He XY, Wu XS, Arun G, Lu B, et al. POU2F3 is a master regulator of a tuft cell-like variant of small cell lung cancer. Genes Dev 2018;32:915–28.
18. Johnson BE, Ihde DC, Makuch RW, Gazdar AF, Carney DN, Oie H, et al. Myc family oncogene amplification in tumor cell lines established from small cell lung cancer patients and its relationship to clinical status and course. J Clin Invest 1987;79:1629–34.
19. Grunblatt E, Wu N, Zhang H, Liu X, Norton JP, Ohol Y, et al. MYCN drives chemoresistance in small cell lung cancer while USP7 inhibition can restore chemosensitivity. Genes Dev 2020;34:1210–26.
20. Jingyao C, Xiangyu P, Feifei N, Xuelan C, Chong C. Epigenetic reprogramming in small cell lung cancer. Cancer Biol Med 2022;19:1111–6.
21. Konieczkowski DJ, Johannessen CM, Abudayyeh O, Kim JW, Cooper ZA, Piris A, et al. A melanoma cell state distinction influences sensitivity to MAPK pathway inhibitors. Cancer Discov 2014;4:816–27.
22. Oser MG, Janne PA. Small-cell neuroendocrine tumors: cell state trumps the oncogenic driver. Clin Cancer Res 2018;24:1775–6.
23. Ireland AS, Micinski AM, Kastner DW, Guo B, Wait SJ, Spainhower KB, et al. MYC drives temporal evolution of small cell lung cancer subtypes by reprogramming neuroendocrine fate. Cancer Cell 2020;38:60–78.e12.
24. Hook KE, Garza SJ, Lira ME, Ching KA, Lee NV, Cao J, et al. An integrated genomic approach to identify predictive biomarkers of response to the aurora kinase inhibitor PF-03814735. Mol Cancer Ther 2012;11:710–9.
25. Dammert MA, Brägelmann J, Olsen RR, Böhm S, Monhasery N, Whitney CP, et al. MYC paralog-dependent apoptotic priming orchestrates a spectrum of vulnerabilities in small cell lung cancer. Nat Commun 2019;10:3485.
26. Huang F, Ni M, Chalishazar MD, Huffman KE, Kim J, Cai L, et al. Inosine monophosphate dehydrogenase dependence in a subset of small cell lung cancers. Cell Metab 2018;28:369–82.